Spin-reorientation transition in $SrNdFeO_4$

2004 J. Phys.: Condens. Matter 16 1823

(http://iopscience.iop.org/0953-8984/16/10/014)

INSTITUTE OF PHYSICS PUBLISHING JOURNAL OF PHYSICS: CONDENSED MATTER

J. Phys.: Condens. Matter **16** (2004) 1823–1836 PII: S0953-8984(04)70635-9

Spin-reorientation transition in $SrNdFeO_4$

Shigeaki Oyama[1], **Makoto Wakeshima**[1], **Yukio Hinatsu**[1] **and Kenji Ohoyama**[2]

[1] Division of Chemistry, Graduate School of Science, Hokkaido University, Sapporo 060-0810, Japan
[2] Institute for Materials Research, Tohoku University, Sendai 980-8577, Japan

Received 14 October 2003
Published 27 February 2004
Online at stacks.iop.org/JPhysCM/16/1823 (DOI: 10.1088/0953-8984/16/10/014)

Abstract

The spin-reorientation transition of layered perovskite oxide $SrNdFeO_4$ has been investigated through powder x-ray and neutron diffraction, magnetic susceptibility, specific heat and ^{57}Fe Mössbauer spectrum measurements. This oxide presents tetragonal symmetry (space group: $I4/mmm$) and the FeO_6 octahedron is axially distorted. Through its magnetic susceptibility and specific heat measurements, two magnetic anomalies were found at around 15 and 36 K. From ^{57}Fe Mössbauer spectra and neutron diffraction profiles of $SrNdFeO_4$, it has been elucidated that the anomalies observed at 15 and 36 K correspond to the antiferromagnetic ordering of the Nd^{3+} ion and a change in the direction of magnetic moment of the Fe^{3+} ion, respectively. The magnetic structures above and below the spin-reorientation transition temperature were determined. The spin-reorientation transition observed in $SrNdFeO_4$ has been induced by the onset of local magnetic interactions between the neodymium and iron sublattices.

1. Introduction

It is known that the K_2NiF_4-type structures [1–3] show interesting physical properties. This structures corresponds to the case for $n = 1$ in the Ruddlesdon–Popper type structure of which the general formula is $AO(ABO_3)_n$ or $A_{n+1}B_nO_{3n+1}$. Whereas ABO_3 perovskites ($n = \infty$) form three-dimensional octahedral networks of corner-shared BO_6 octahedra, the ideal tetragonal K_2NiF_4-type structures are composed of alternating perovskite ABO_3 and rock salt AO layers along the tetragonal c axis. Hence, the important feature of the K_2NiF_4-type structures is B–O–B bonds of two-dimensional corner-sharing octahedral networks in the perovskite ABO_3 structure, and the compounds with this structure have two-dimensional magnetic properties.

The layered perovskite type oxide $SrLnFeO_4$ (Ln = lanthanides) is crystallized in the ideal tetragonal K_2NiF_4-type structure with space group $I4/mmm$ [4–6]. These oxides were

prepared for Ln = La, Pr, Nd, Sm, Eu, Gd, Tb and Dy and characterized by means of x-ray diffraction. Previous investigations show that the magnetic moments of Fe^{3+} ions in these oxides have an antiferromagnetic arrangement below 250–400 K [7, 8]. Early ^{57}Fe Mössbauer spectra measurements on the $SrLnFeO_4$ samples with Ln = Pr, Nd indicate that the spin reorientation of the Fe^{3+} moments may occur [9] but details were not reported. Recently, it was observed that the direction of the net magnetic moment in $LnFeO_3$ rotates continuously or abruptly from one crystallographic axis to another due to the antisymmetric and anisotropic-symmetric exchange interactions between Fe^{3+} and Ln^{3+} [10].

In this study, we have paid attention to the spin-reorientation transition of the layered perovskite type oxide, $SrNdFeO_4$, because the contribution of Nd^{3+} ions to the change of direction of Fe^{3+} moments has not been reported yet. Some interesting magnetic anomalies have been found through powder neutron diffraction, magnetic susceptibility, specific heat and ^{57}Fe Mössbauer spectra measurements and their results are discussed here.

2. Experimental details

The polycrystalline sample $SrNdFeO_4$ was prepared by the standard solid-state reaction. As starting materials, strontium carbonate $SrCO_3$, neodymium sesquioxide Nd_2O_3 and diiron trioxide Fe_2O_3 were used. Nd_2O_3 was dried in advance at 1173 K before use. These reagents were weighed in appropriate metal ratios and ground intimately in an agate mortar. The mixtures were pressed into pellets and then calcined in a flow of argon gas at 1273 K for 12 h. After being cooled to room temperature, the pellets were reground, repressed and heated in a flow of argon gas at 1723 K for 48 h with regrinding and repelletizing.

The powder x-ray diffraction measurements were carried out at room temperature in the range of $10^\circ \leqslant 2\theta \leqslant 120^\circ$ using a 2θ step size of 0.02° with Cu Kα radiation on a MultiFlex diffractometer (Rigaku, Japan). The structure refinement was carried out by Rietveld analysis for the powder x-ray diffraction data with the program RIETAN2000 [11].

The powder neutron diffraction measurements were carried out at 2, 5, 10, 15, 20, 25, 30, 34, 40 and 100 K, and at room temperature, in the range of $3^\circ \leqslant 2\theta \leqslant 153^\circ$ at intervals of 0.1° with a wavelength of 1.8207 Å. Measurements were performed on the Kinken powder diffractometer for high efficiency and high resolution measurements, HERMES, of the Institute for Materials Research (IMR), Tohoku University [12], installed at the JRR-3M Reactor at the Japan Atomic Energy Research Institute (JAERI), Tokai. The magnetic structures were determined by the Rietveld technique, using the program FullProf [13].

Magnetic susceptibility measurements were made using a SQUID magnetometer (Quantum Design, MPMS model). Susceptibility–temperature curves for each sample were measured under both the ZFC (zero-field-cooled) and FC (field-cooled) conditions. The former was measured on heating the sample to 400 K after zero-field cooling to 1.8 K, applying a field of 1000 G. The latter was measured on cooling from 400 to 1.8 K at 1000 G.

Specific heat measurements were made using a relaxation technique with a heat capacity measurement system (Quantum Design, PPMS model) in the temperature range from 1.8 to 300 K. The sintered sample in the form of a pellet was mounted on a sample holder with Apiezon grease for better thermal contact.

The ^{57}Fe Mössbauer spectra were measured at 15, 20, 25, 30, 35, 40, 45, 50, 70, 100, 200, 300, 320, 340, 360 and 400 K with a conventional transmission Mössbauer spectrometer VT-6000 (Laboratory Equipment Co.) in the constant acceleration mode. Absorbers were prepared of finely ground $SrNdFeO_4$ which was weighed to give the optimum signal-to-noise ratio. A source of up to 100 mCi of ^{57}Co in Rh was used and the spectrometers were calibrated using α-iron at room temperature.

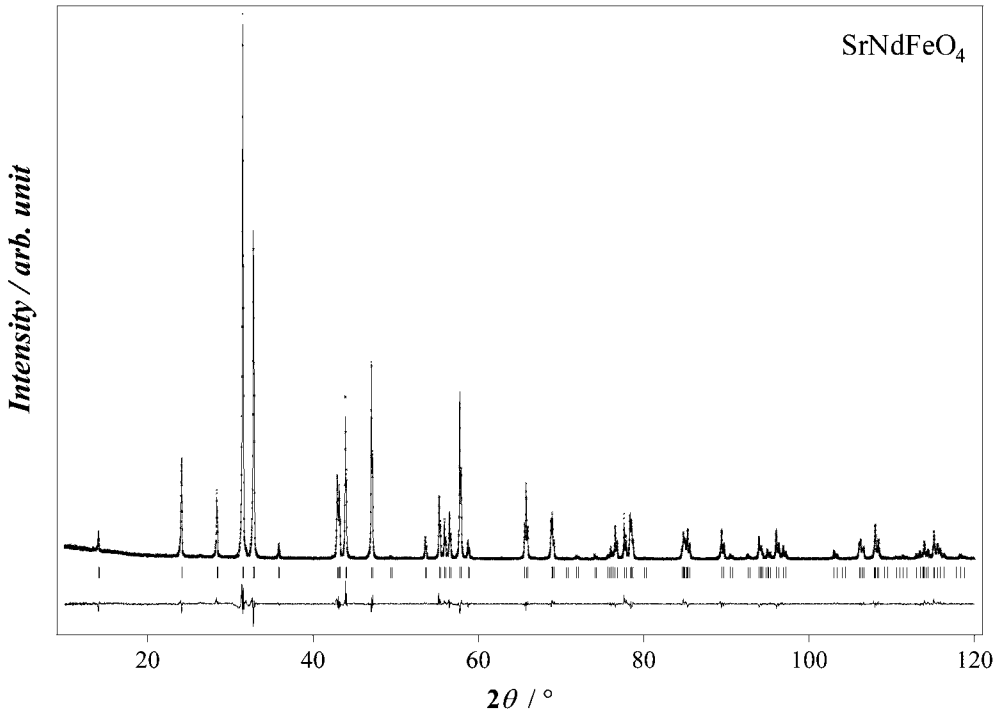

Figure 1. X-ray diffraction profiles for $SrNdFeO_4$. The calculated and observed diffraction profiles are shown by the top full curve and the cross markers, respectively. The vertical markers in the middle show positions calculated for Bragg reflections. The lower trace is a plot of the difference between calculated and observed intensities.

3. Results and discussion

3.1. Crystal structures

The results of the x-ray diffraction measurements show that $SrNdFeO_4$ was found to form in a single phase. Its x-ray diffraction patterns are shown in figure 1 and the data have been analysed by the Rietveld method. The result indicates that $SrNdFeO_4$ has an ideal tetragonal K_2NiF_4-type structure (space group: $I4/mmm$) in which Sr^{2+} and Nd^{3+} ions are randomly distributed at the same Wyckoff 4e positions. The structural parameters obtained from Rietveld refinements are summarized in table 1 and the crystal structure of $SrNdFeO_4$ is illustrated in figure 2. In an ideal tetragonal K_2NiF_4-type structure, the strontium and neodymium atoms are nine-fold-coordinated and the iron atom is six-fold-coordinated. Furthermore, the coordination polyhedrons have three and two different interatomic distances, respectively, because the oxygen atoms are fully occupied at two different 4c $(0, 1/2, 0)$ and 4e $(0, 0, z)$ sites in this structure. The selected interatomic distances are summarized in table 2. The iron is coordinated by six oxygen atoms forming an elongated FeO_6 octahedron, which has four in-plane Fe–O bonds (1.928 Å) and two axial Fe–O bonds (2.121 Å). This indicates that the FeO_6 octahedron is strongly axially distorted, which results in the existence of a large electric quadrupole interaction.

3.2. Magnetic properties

Figure 3 shows the temperature dependence of the magnetic susceptibility between 1.8 and 400 K. In the inset of figure 3, the temperature dependence of the reciprocal susceptibility is

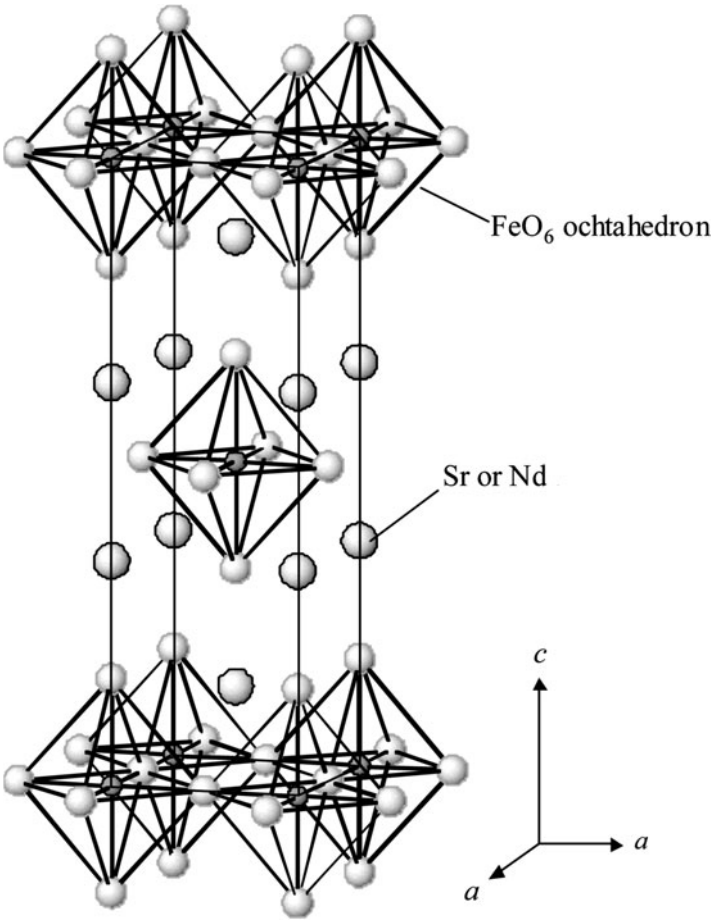

Figure 2. The crystal structure of $SrNdFeO_4$. Spheres are Sr or Nd atoms and octahedra are FeO_6 units.

Table 1. Structural parameters of $SrNdFeO_4$ at room temperature obtained from Rietveld refinement of the x-ray diffraction data. (Note: $R_{wp} = [\sum w(|F(obs)| - |F(cal)|)^2 / \sum w|F(obs)|^2]^{1/2}$, $R_I = \sum |I_k(obs) - I_k(cal)| / \sum I_k(obs)$ and $R_F = \sum |[I_k(obs)]^{1/2} - [I_k(cal)]^{1/2}| / \sum [I_k(obs)]^{1/2}$.)

Atom	Site	Occupation	x	y	z	B (Å^2)
Sr, Nd	4e	1.0	0	0	0.3585(1)	0.13(2)
Fe	2a	1.0	0	0	0	0.02(4)
O(1)	4c	1.0	0	0.5	0	1.01(1)
O(2)	4e	1.0	0	0	0.1689(4)	1.01(1)

Space group: $I4/mmm$ (No. 139)

$a = 3.8556(2)$ Å, $c = 12.5586(8)$ Å, $V = 186.69(2)$ Å^3
$R_{wp} = 11.45\%$, $R_I = 3.13\%$, $R_F = 2.13\%$

shown. In the temperature range of 360–400 K, which is higher than T_N (=360 K) of the Fe^{3+} sublattice, the magnetic susceptibility was fitted with a Curie–Weiss law. The effective magnetic moment obtained in this temperature range is 6.38(5) μ_B, which is lower than that

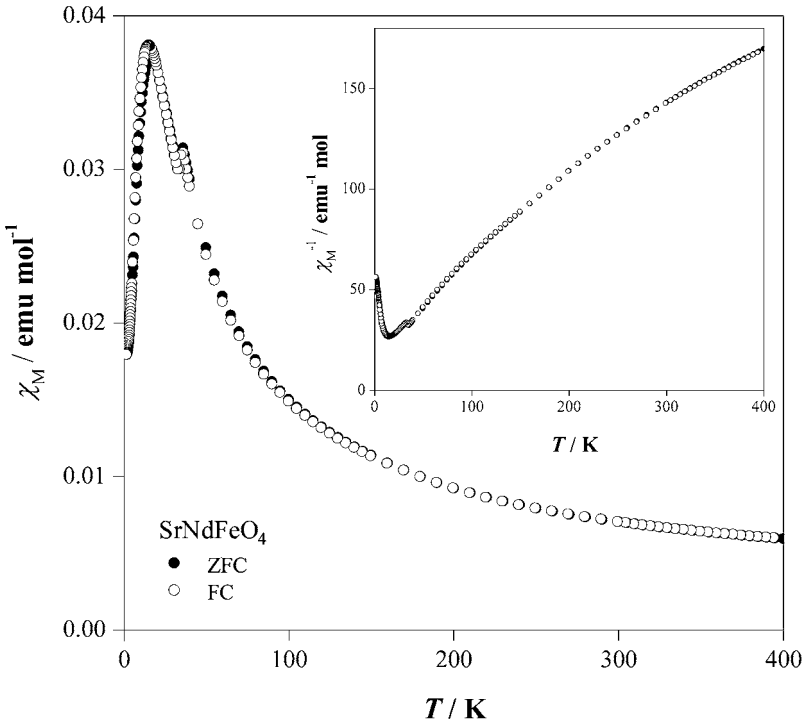

Figure 3. Temperature dependence of the magnetic susceptibility of $SrNdFeO_4$. The reciprocal susceptibility is shown in the inset.

Table 2. Selected interatomic distances (Å) at room temperature.

Sr, Nd–O(1)	×4	2.622(1)
Sr, Nd–O(2)	×1	2.381(5)
Sr, Nd–O(2)	×4	2.748(2)
Fe–O(1)	×4	1.928(1)
Fe–O(2)	×2	2.121(5)
Fe–O(2)/Fe–O(1)		1.100

expected for the paramagnetic contribution of free Nd^{3+} and Fe^{3+} ions, i.e. 6.94 μ_B. This reduction in the effective magnetic moment should be due to two-dimensional correlations in the layered Fe^{3+} sublattice. This is emphasized by the magnetic susceptibility of $SrLaFeO_4$ that depends only on the magnetic behaviour of Fe^{3+} ions [8] and is characteristic of the K_2NiF_4-type structure. To investigate the correct effective magnetic moment the measurements of the magnetic susceptibility at the higher temperatures may be needed.

In the plot of the magnetic susceptibility against temperature, two marked anomalies have been observed. The magnetic susceptibility shows a maximum at 15 K and decreases rapidly with decreasing temperature below this temperature, indicating the occurrence of an antiferromagnetic transition. Since the magnetic moments of the Fe^{3+} sublattice have already been ordered above this temperature (at 360 K), an antiferromagnetic transition observed at 15 K may be due to the magnetic ordering of the Nd^{3+} moments. This is in contrast to the result of the magnetic susceptibility measurement on the similar K_2NiF_4-type oxide $CaNdCrO_4$, which indicates the appearance of short-range magnetic correlations of the antiferromagnetic

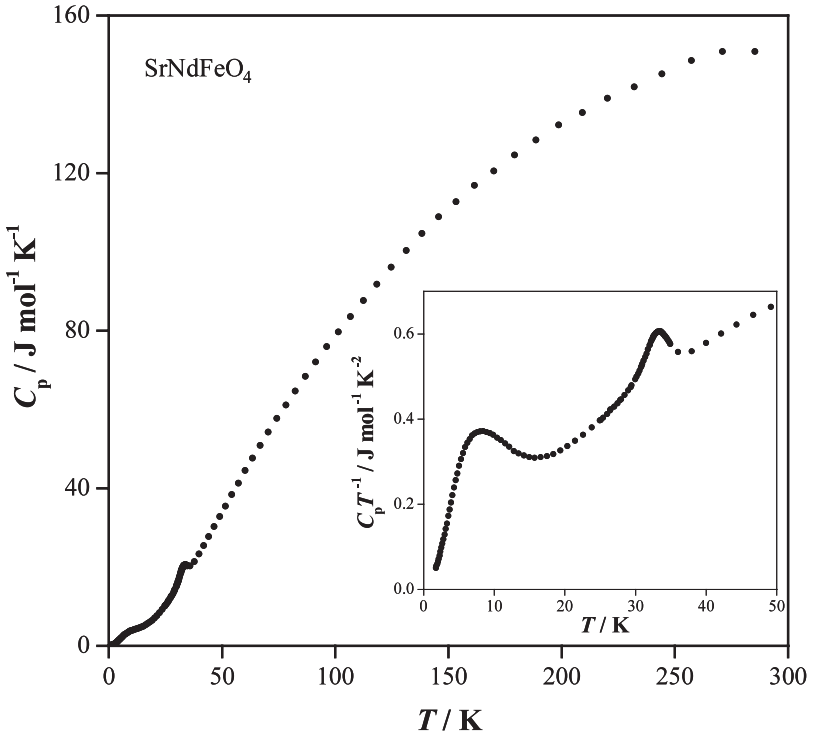

Figure 4. Temperature dependence of the specific heat (C_p) of $SrNdFeO_4$. The $C_pT^{-1} - T$ curve is shown in the inset.

characteristic within the Nd^{3+} sublattice [14]. On the other hand, our experiments show that $SrNdFeO_4$ has a long-range magnetic interaction, which is interesting from the fact that three-dimensional magnetic ordering involving the Nd^{3+} ions is not favoured by the chemical disorder (Sr^{2+}, Nd^{3+}) at the 4e sites. The existence of a long-range magnetic ordering within the Nd^{3+} sublattice has been elucidated by the neutron diffraction measurements.

$SrNdFeO_4$ shows another magnetic anomaly at 36 K in its susceptibility versus temperature curve (figure 3). To clear this anomaly, specific heat measurements have been performed. Figure 4 shows the variation of the specific heat for $SrNdFeO_4$ as a function of temperature. The specific heat measurements show two broad anomalies at 15 and 36 K, which corresponds to the magnetic anomalies found in the magnetic susceptibility measurements. This fact indicates that the magnetic transitions occur at these temperatures. The transition at 15 K is an antiferromagnetic transition of the Nd^{3+} ions. The magnetic transition at 36 K is due to the spin reorientation of the Fe^{3+} magnetic moments [7], as described later.

3.3. ^{57}Fe *Mössbauer spectra*

Figure 5 shows the ^{57}Fe Mössbauer spectra of $SrNdFeO_4$ at 15, 35, 40, 340 and 400 K. Two absorption peaks in the spectrum measured at 400 K show that the Fe^{3+} ion is in a paramagnetic state, whereas six absorption peaks appeared in the other spectra measured below 340 K indicate the antiferromagnetic ordering of the Fe^{3+} ion. In $SrNdFeO_4$, the Fe^{3+} ions occupy the 2a sites (space group: $I4/mmm$) with a crystallographic tetragonal point group $4/mmm$ and one can expect the existence of an electric quadrupole interaction between the electric field gradient

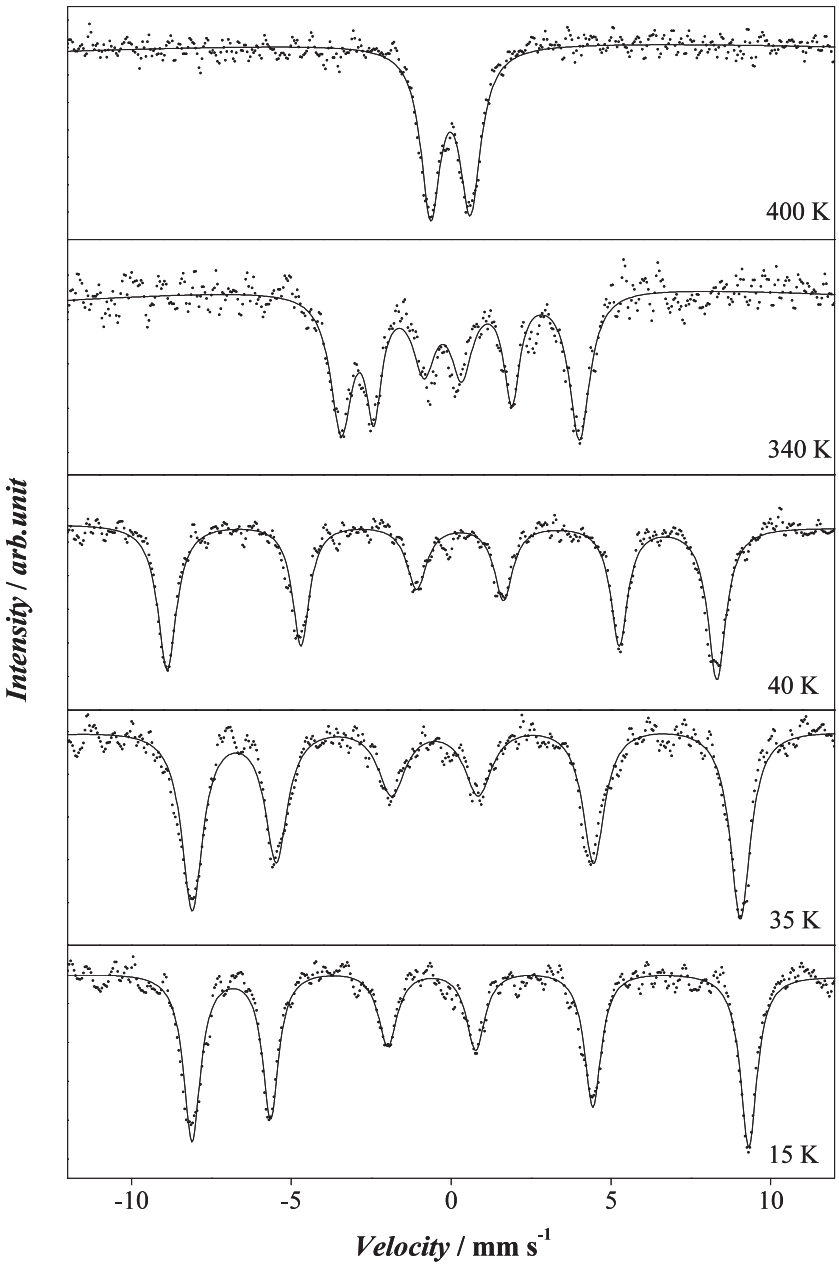

Figure 5. ^{57}Fe Mössbauer spectra of $SrNdFeO_4$ at 15, 35, 40, 340 and 400 K.

and the electric quadrupole moment of the Fe^{3+} ions. Therefore, each of the spectra measured between 15 and 340 K can be fitted with six Lorentzians containing this interaction.

In $SrNdFeO_4$, the isomer shift δ of Fe^{3+} at 300 K is determined to be 0.16(1) mm s^{-1}. Since the isomer shifts for the high-spin ($S = 5/2$) compounds of Fe^{3+} with the electronic configuration of [Ar]$3d^5$ ([Ar]: argon electronic core) are generally 0.15–0.5 mm s^{-1}, the value obtained at this temperature is appropriate and comparable with the isomer shift of

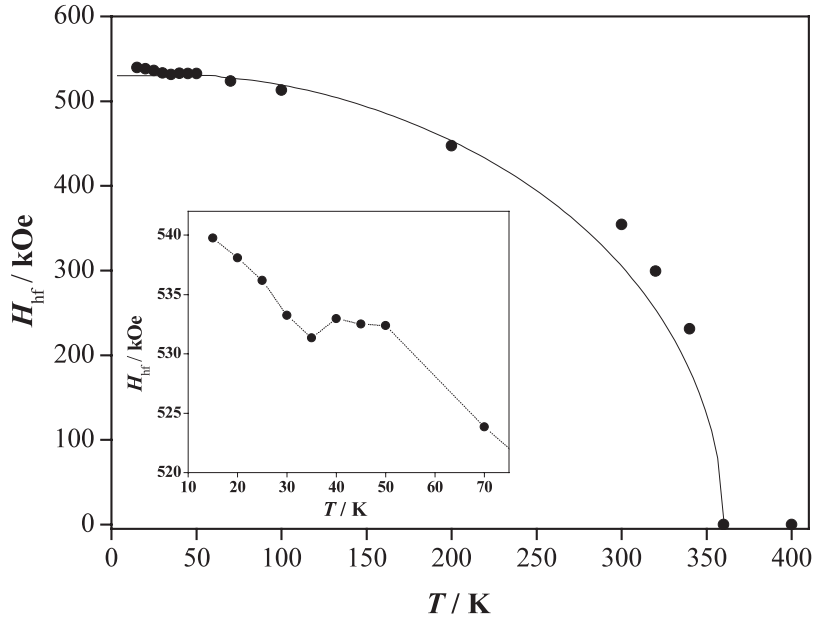

Figure 6. Temperature dependence of the magnetic hyperfine field of $SrNdFeO_4$.

$SrNd_2Fe_2O_7$ at room temperature having the Ruddlesdon–Popper type oxide ($n = 2$) with high-spin Fe^{3+}, 0.105 mm s^{-1} [15].

Figure 6 shows the temperature dependence of the magnetic hyperfine field determined for $SrNdFeO_4$ between 15 and 400 K. As seen in the figure, the H_{hf} versus T curve can be roughly reproduced by the Brillouin function for $S = 5/2$. The magnetic ordering temperature of the Fe^{3+} sublattice in this compound is estimated to be about 360 K. The magnetic hyperfine field deduced at 0 K is 540 kOe, which is appropriate for the Fe^{3+} ion at the high spin state. As shown in the inset of figure 6, the abnormal change of the H_{hf} versus T curve has been observed at 35 K, i.e. the magnetic hyperfine field once increases with temperature above this temperature. This behaviour corresponds to the anomalies observed in the magnetic susceptibility and specific heat measurements. We consider that the above-mentioned abnormal variation of the magnetic hyperfine field with temperature is due to the occurrence of the spin-reorientation of the magnetic moments of the Fe^{3+} ions at 35 K.

Figure 7 shows the temperature dependence of the electric quadrupole splitting parameters (Δ) in the temperature range between 15 and 400 K. The large quadrupole splitting parameter shows that Fe^{3+} ions are in an asymmetric local environment coordinated by six oxygen atoms. The quadrupole splitting parameters against temperature indicate that there exist three kinds of spin states for Fe^{3+} ions, depending on temperature. Above 360 K, the Fe^{3+} ions are in the paramagnetic state which gives $\Delta \sim 1.2$ mm s^{-1}. In the temperature region between 35 and 360 K, the Fe^{3+} ions are in the antiferromagnetic state which gives $\Delta \sim -0.6$ mm s^{-1}. Below 35 K, the quadrupole splitting parameter is $\Delta \sim 1.2$ mm s^{-1}.

In the paramagnetic region, the quadrupole splitting is given by the following equation [16]:

$$\Delta = \tfrac{1}{2}e^2qQ(1 + \tfrac{1}{3}\eta^2)^{\frac{1}{2}}, \tag{1}$$

where eq is the value of the electric field gradient (EFG) along the maximum principal axis of EFG, Q is the nuclear quadrupole moment and η is the asymmetry parameter of the EFG. Here, in an ideal tetragonal K_2NiF_4-type structure, EFG of the B site cation must be axially

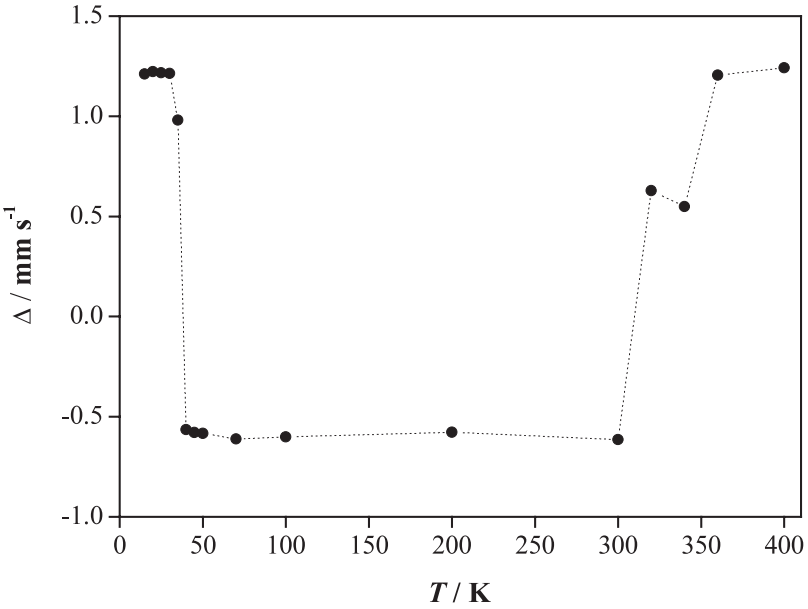

Figure 7. Temperature dependence of the electric quadrupole splitting (Δ) of $SrNdFeO_4$.

symmetric, so that the asymmetry parameter η equals zero. Therefore, the equation (1) is simplified as follows:

$$\Delta = \tfrac{1}{2} e^2 q\, Q. \tag{2}$$

Below the Néel temperature, when the principal axis makes an angle θ with the magnetic axis, the effective quadrupole interaction (Δ_{eff}) can be described in the following [17]:

$$\Delta_{\text{eff}} = \frac{e^2 q\, Q}{2}\left(\frac{3\cos^2\theta - 1}{2}\right) = \Delta\left(\frac{3\cos^2\theta - 1}{2}\right). \tag{3}$$

The angle θ is not determinable from the Mössbauer spectrum in the magnetic–quadrupole interaction, so that $e^2 q\, Q$ cannot be calculated unless the direction of magnetization relative to the symmetry axis is measured by other means.

As shown in figure 7, the values of the quadrupole splitting changes largely from positive to negative when the temperature is increased through 35 K, which shows the occurrence of the spin-reorientation transition of the Fe^{3+} magnetic moments at this temperature. From equation (3), it has been found that the quadrupole splitting parameter $\Delta \sim -0.6$ mm s^{-1} in the temperature range between 35 and 360 K corresponds to $\theta = 90°$ and that of $\Delta \sim 1.2$ mm s^{-1} in the temperature region below 35 K corresponds to $\theta = 0°$. This result indicates that the direction of magnetic moment of the Fe^{3+} ion should rotate by 90° at 35 K. In order to elucidate the direction of magnetic moment of the Fe^{3+} ion, the magnetic structures of $SrNdFeO_4$ above and below the spin-reorientation temperature were determined through the powder neutron diffraction measurements.

3.4. Magnetic structures

Neutron diffraction data were collected in the temperature range between 2 K and room temperature. The diffraction profiles at 2 and 40 K are shown in figure 8. In all the diffraction

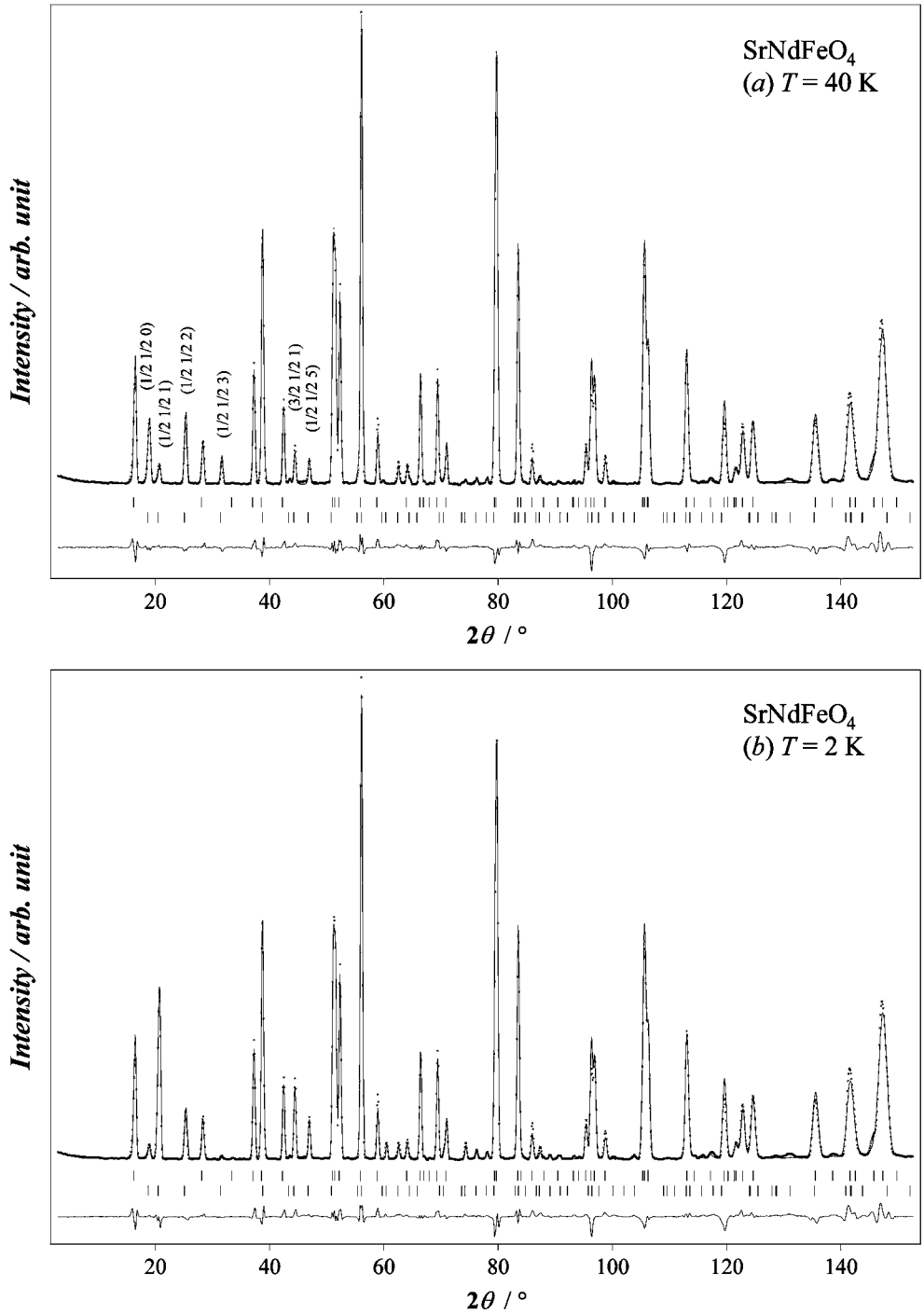

Figure 8. Powder neutron diffraction profiles for $SrNdFeO_4$ at 40 (a) and 2 K (b). The calculated and observed diffraction profiles are shown by the top full curve and the cross markers, respectively. The nuclear reflection positions are shown as upper vertical markers and magnetic ones are shown as lower ones. The lower trace is a plot of the difference between calculated and observed intensities.

Table 3. Crystal and magnetic data determined by neutron diffraction measurements at 40 and 2 K for $SrNdFeO_4$. (Note: $R_{wp} = [\sum w(|F(obs)| - |F(cal)|)^2 / \sum w|F(obs)|^2]^{1/2}$, $R_{Bragg} = \sum |I(obs) - I(cal)| / \sum I(obs)$ and $R_{mag} = \sum |I_{mag}(obs) - I_{mag}(cal)| / \sum I_{mag}(obs)$.)

	Site	x	y	z	B (Å^2)
			40 K		
Sr, Nd	4e	0	0	0.3591(2)	0.02(8)
Fe	2a	0	0	0	0.35(2)
O(1)	4c	0	0.5	0	1.61(2)
O(2)	4e	0	0	0.1709(1)	1.61(2)
			2 K		
Sr, Nd	4e	0	0	0.3589(7)	0.01(3)
Fe	2a	0	0	0	0.25(4)
O(1)	4c	0	0.5	0	1.56(5)
O(2)	4e	0	0	0.1705(1)	1.56(5)
Space group: $I4/mmm$ (No. 139)					
40 K					
$R_{wp} = 12.4\%$, $R_{Bragg} = 6.37\%$, $R_{mag} = 16.1\%$ $a = 3.8491(8)$ Å, $c = 12.4822(6)$ Å m (Fe^{3+}) $= 4.11(9)$ μ_B					
2 K					
$R_{wp} = 13.2\%$, $R_{Bragg} = 6.74\%$, $R_{mag} = 17.6\%$ $a = 3.8494(9)$ Å, $c = 12.4805(3)$ Å m (Fe^{3+}) $= 4.23(9)$ μ_B, m (Nd^{3+}) $= 2.45(1)$ μ_B					

profiles below room temperature, magnetic Bragg reflections $\{h/2\ k/2\ l\}$ with $h, k =$ odd appeared. This result indicates that the magnetic moments of the Fe^{3+} ions in the $SrNdFeO_4$ compound has a long-range magnetic ordering and that its magnetic structure has dimensions $\sqrt{2}a \times \sqrt{2}a \times c$ in terms of the tetragonal chemical cell (propagation vector of $\boldsymbol{k} = [1/2\ 1/2\ 0]$). Figure 9 shows the temperature dependence of the integrated intensities of some magnetic Bragg reflections. A discontinuous change of the intensities suggests that a magnetic phase transition occurs at around 40 K, which is attributable to the spin reorientation of the Fe^{3+} moments observed through the magnetic susceptibility, specific heat and Mössbauer spectrum measurements.

We refined the magnetic structure from the diffraction profiles by the Rietveld method using the magnetic structure model with the propagation vector of $\boldsymbol{k} = [1/2\ 1/2\ 0]$. The magnetic structure below 35 K is that the directions of both the magnetic moments of Nd^{3+} and Fe^{3+} ions are pointing along the $\langle 001 \rangle$ direction. On the other hand, the best fit for the profiles above 40 K indicates that only the Fe moments are parallel to the $\langle 110 \rangle$ direction and the Nd moments make no contribution to the magnetic Bragg reflections. Table 3 lists the refined crystallographic and magnetic parameters at 2 and 40 K. Figure 10 illustrates the magnetic structures above 40 K and below 35 K. For determining the magnetic structure above 40 K, we assumed that all the spins are collinear, because our measurements cannot distinguish between noncollinear and collinear structure models [18]. Recently, Kawanaka *et al* [19] reported that the Fe^{3+} spins in $SrLaFeO_4$ lie in the $\langle 110 \rangle$ direction through the magnetization measurements by using a single crystal. From this result, we believe that the magnetic structure above 40 K for $SrNdFeO_4$ is the collinear one.

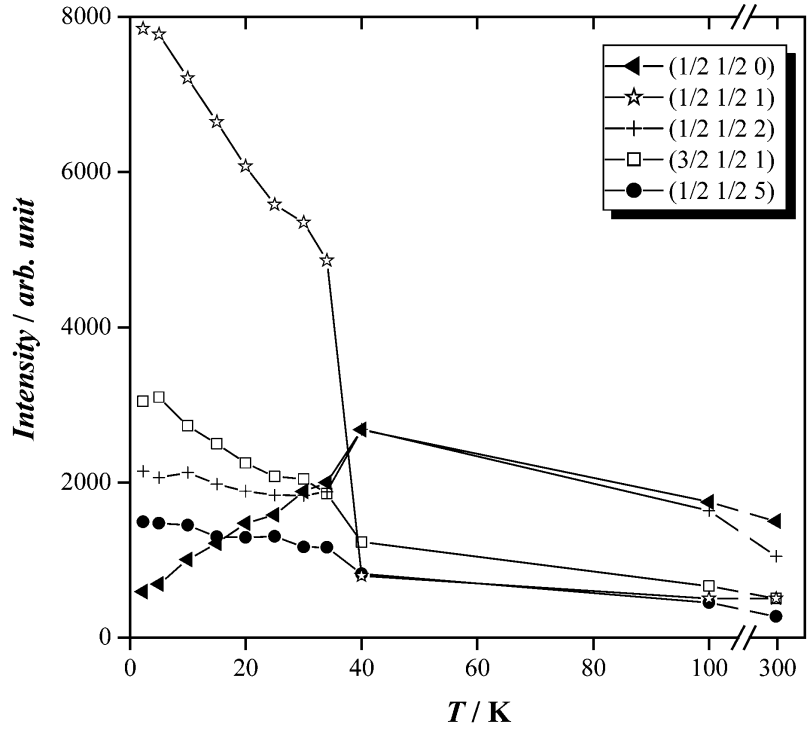

Figure 9. Temperature dependence of the integrated intensities of some magnetic Bragg reflections for $SrNdFeO_4$.

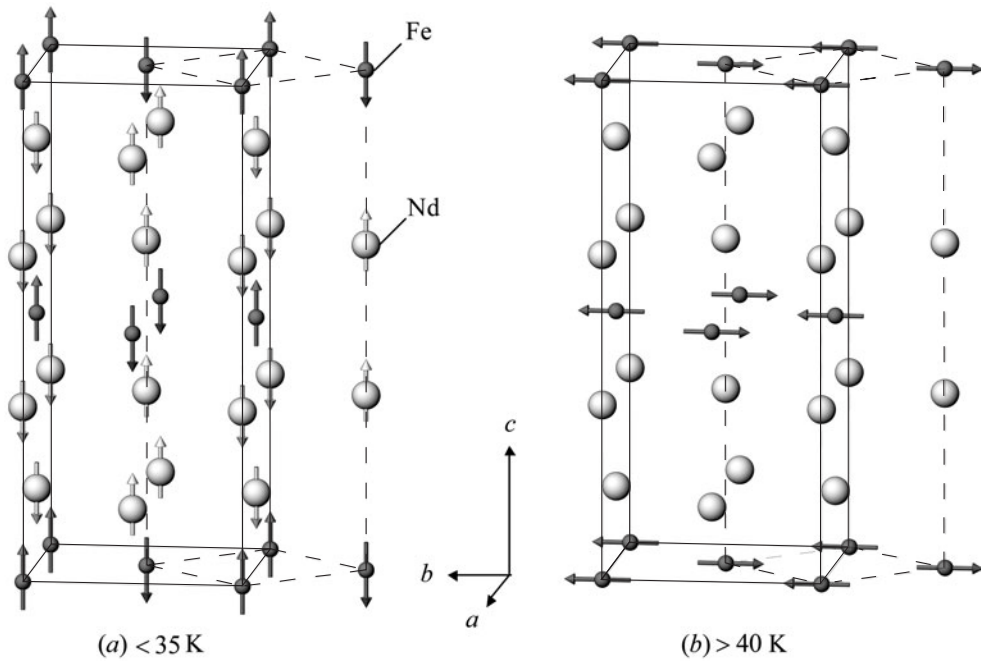

Figure 10. Magnetic structure models of $SrNdFeO_4$ below 35 K (a) and above 40 K (b). Diamagnetic ions are omitted. Arrows show the direction of the magnetic moments.

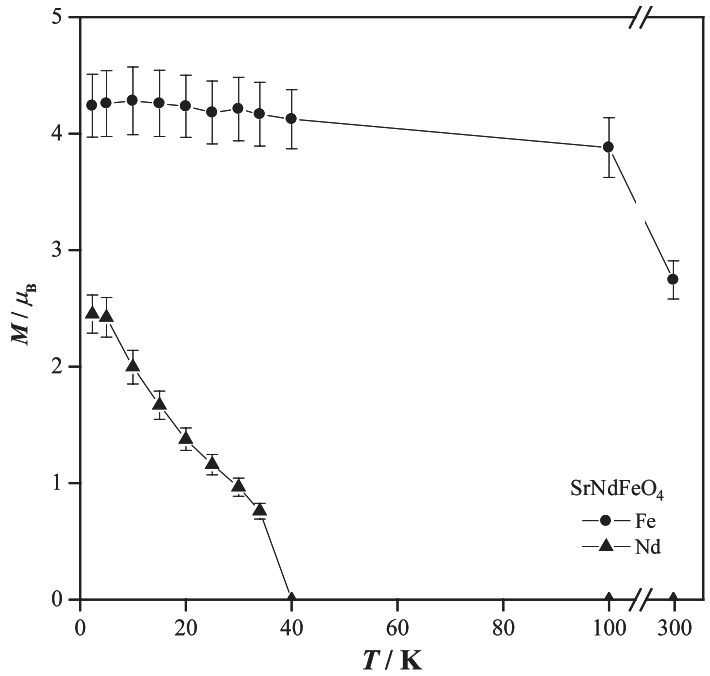

Figure 11. Temperature dependence of the ordered magnetic moments of Fe^{3+} and Nd^{3+} ions.

In the collinear structural model, the Fe^{3+} moments lie on the *ab* plane above 40 K and turn to the *c* direction below 35 K. Such a 90° rotation of the Fe^{3+} moments from the *b* direction to the *c* direction is consistent with the conclusion from the change of the magnetic–quadrupole interaction with temperature in the Mössbauer measurements. Furthermore, in the magnetic structure below 35 K the directions of the Fe^{3+} magnetic moments and Nd^{3+} magnetic moments are collinear, which bears out the local magnetic interactions between Nd^{3+} and Fe^{3+} ions [20].

Figure 11 shows the temperature dependence of the ordered magnetic moments of Fe^{3+} and Nd^{3+} ions determined by the Rietveld refinement for the neutron diffraction data. From this figure, it has been found that the ordered magnetic moments of Fe^{3+} ions increases with decreasing temperature and are almost constant (at about 4.2 μ_B) below 40 K. This behaviour corresponds to the variation of the magnetic hyperfine field against temperature (see figure 6). On the other hand, the ordered magnetic moments of Nd^{3+} appear below 35 K, increase rapidly below about 20 K with decreasing temperature and reach to 2.45(1) μ_B at 2 K. The beginning of the rapid increase corresponds to the broad maximum (about 15 K) in the χ versus T and C_p versus T curves. The low value of the Nd^{3+} moment at 2 K, compared with the theoretical moment of 3.27 μ_B ($g_J = 8/11$, $J = 9/2$), should be due to the crystal field effect [18]. It is worth noting that the temperature at which the Nd^{3+} moments magnetically order coincides with the spin-reorientation transition temperature of Fe^{3+} moments. This fact indicates that the spin reorientation of the Fe^{3+} sublattices could be induced by the onset of local magnetic interactions between Nd^{3+} and Fe^{3+} ions.

References

[1] Balz D and Pleith K 1955 *Z. Elektrochem.* **59** 545
[2] Birgeneau R J, Guggenheim H J and Shirane G 1969 *Phys. Rev. Lett.* **22** 720
[3] Birgeneau R J, DeRosa F and Guggenheim H J 1970 *Solid State Commun.* **8** 13

[4] Blasse G 1965 *J. Inorg. Nucl. Chem.* **27** 2685
[5] Joubert J C, Collomb A, Elmaleh D, Le Flem G, Daoudi A and Olliver G 1970 *J. Solid State Chem.* **2** 343
[6] Kim M G, Ryu K H and Yo C H 1996 *J. Solid State Chem.* **123** 161
[7] Shimada M and Koizumi M 1976 *Mater. Res. Bull.* **11** 1237
[8] Soubeyroux J L, Courbin P, Fournes L, Fruchart D and Le Flem G 1980 *J. Solid State Chem.* **31** 313
[9] Shimada M, Koizumi K, Takano M, Shinjo T and Takada T 1979 *J. Physique* **40** 272
[10] Saito K, Yamamura Y, Mayer J, Kobayashi H, Miyazaki Y, Ensling J, Gütlich p, Leśniewska B and Sorai M 2001 *J. Magn. Magn. Mater.* **225** 381
[11] Izumi F and Ikeda T 2000 *Mater. Sci. Forum* **198** 321
[12] Ohoyama K, Kanouchi T, Nemoto K, Ohashi M, Kajitani T and Yamaguchi Y 1998 *Japan. J. Appl. Phys.* **37** 3319
[13] Rodriguez-Carvajal J 1993 *Physica* B **192** 55
[14] Romero de Paz J, Hernández Velacco J, Fernández-Díaz M T, Porcher P, Martínez J L and Sáez Puche R 1999 *J. Solid State Chem.* **148** 361
[15] Samaras D and Chevalier R 1977 *J. Magn. Magn. Mater.* **5** 35
[16] Uhm Y R and Kim C S 2001 *J. Appl. Phys.* **89** 7344
[17] Hector A L, Hutchings J A, Needs R L, Thomas M F and Weller M T 2001 *J. Mater. Chem.* **11** 527
[18] Matsuda M, Yamada K, Kakurai K, Kadowaki H, Thurston T R, Endoh Y, Hidaka Y, Birgeneau R J, Kastner M A, Gehring P M, Moudden A M and Shirane G 1990 *Phys. Rev.* B **42** 10098
[19] Kawanaka H, Bando H, Mitsugi K, Sasahara A and Nishihara Y 2004 *Physica* B **329–333** 797
[20] Sachidanandam R, Yildirim T, Harris A B, Aharony A and Entin-Wohlman O 1997 *Phys. Rev.* B **56** 260